Large Pore Methylene-Bridged Periodic Mesoporous Organosilicas: Synthesis, Bifunctionalization and Their Use as Nanotemplates

Wen-Hua Zhang,[†] Brian Daly,[†] John O'Callaghan,[†] Lei Zhang,[‡] Jian-Lin Shi,[§] Can Li,[‡] Michael A. Morris,[†] and Justin D. Holmes*[,†]

Department of Chemistry, Materials Section and Supercritical Fluid Centre, University College Cork, Cork, Ireland, Centre for Research on Adaptive Nanostructures and Nanodevices (CRANN), Trinity College Dublin, Dublin, Ireland, State Key Laboratory of Catalysis, Dalian Institute of Chemical Physics, Chinese Academy of Sciences, 457 Zhongshan Road, Dalian 116023, P. R. China, and State Key Laboratory of High Performance Ceramics and Superfine Microstructure, Shanghai Institute of Ceramics, Chinese Academy of Sciences, 1295 Ding-Xi Road, Shanghai 200050, P. R. China

Received March 5, 2005. Revised Manuscript Received September 2, 2005

Large pore, methylene-bridged, periodic mesoporous organosilicas (PMO-Me's) have been synthesized using the nonionic surfactant P123 ($EO_{20}PO_{70}EO_{20}$) as a structure-directing agent under acidic conditions. The morphology of the PMO-Me materials was observed to be strongly dependent on the acidity of the solution used in each preparation. Modification of the PMO-Me surface with 3-mercaptopropyltrimethoxysilane (MPTS), via a supercritical fluid grafting reaction, resulted in the formation of a bifunctionalized organosilica (SH-PMO-Me). These SH-PMO-Me materials, coated with Au clusters, were subsequently utilized as templates for the supercritical fluid deposition of germanium nanocrystals. The highly hydrophobic surfaces of the SH-PMO-Me templates, and the effective penetrating power of the supercritical fluid, resulted in rapid diffusion of the germanium precursor into the mesopores to produce highly crystalline nanoparticles and nanorods. These nanocomposite materials were found to be significantly more crystalline than those formed from functionalized Au-coated mesoporous silica templates (SH-SBA-15), highlighting the benefits of using PMOs as hosts for the encapsulation of semiconductor nanomaterials.

Introduction

Ordered mesoporous materials (OMMs), first discovered by researchers at the Mobil Corporation in 1992,[1] have attracted considerable interest due to their potential applications in areas such as catalysis, adsorption, environmental cleanup, drug delivery, nanoelectronics, and polymer mesofibers.[2−4] In particular, the highly ordered and size-tunable channels within OMMs make them ideal hosts for the encapsulation of nanomaterials,[5−8] i.e., nanoparticles,[6] nanowires,[7] and carbon nanotube networks.[8] Mesoporous silica is the most commonly used host for nanocrystal templating, and there have been few reports of inclusion in other types of OMMs.[9]

Periodic mesoporous organosilicas (PMOs) are an attractive class of OMMs.[10] Unlike mesoporous silicas, possessing SiO_2 frameworks, PMOs consist of hybrid structural units, i.e., $-[_{1.5}OSi-R-SiO_{1.5}]-$ (where R is a bridged group, such as $-CH_2CH_2-$, $-CH=CH-$, or phenyl). The inorganic and

* To whom correspondence should be addressed. Phone: +353 (0)21 4903608. Fax: +353 (0)21 4274097. E-mail: j.holmes@ucc.ie.

† University College Cork and Trinity College Dublin.

‡ State Key Laboratory of Catalysis, Dalian Institute of Chemical Physics, Chinese Academy of Sciences.

§ State Key Laboratory of High Performance Ceramics and Superfine Microstructure, Shanghai Institute of Ceramics, Chinese Academy of Sciences.

(1) (a) Kresge, C. T.; Leonowicz, M. E.; Roth, W. J.; Vartuli, J. C.; Beck, J. S. *Nature* **1992**, *359*, 710. (b) Beck, J. S.; Vartuli, J. C.; Roth, W. J.; Leonowicz, M. E.; Kresge, C. T.; Schmitt, K. D.; Chu, C. T. W.; Olson, D. H.; Sheppard, E. W.; McCullen, S. B.; Higgins, J. B.; Schlenker, J. L. *J. Am. Chem. Soc.* **1992**, *114*, 10834.

(2) For reviews, please see: (a) Corma, A. *Chem. Rev.* **1997**, *97*, 2373. (b) Ying, J. Y.; Mehnert, C. P.; Wong, M. S. *Angew. Chem., Int. Ed.* **1999**, *38*, 56. (c) Linssen, T.; Cassiers, K.; Cool, P.; Vansant, E. F. *Adv. Colloid Interface Sci.* **2003**, *103*, 121.

(3) (a) Zhao, D. Y.; Feng, J. L.; Huo, Q. S.; Melosh, N.; Fredrickson, G. H.; Chmelka, B. F.; Stucky, G. D. *Science* **1998**, *279*, 548. (b) Huo, Q.; Margolese, D. I.; Ciesla, U.; Feng, P.; Gier, T. E.; Sieger, P.; Leon, R.; Petroff, P. M.; Schüth, F.; Stucky, G. D. *Nature* **1994**, *368*, 317. (c) Tanev, P. T.; Pinnavaia, T. J. *Science* **1995**, *267*, 865.

(4) (a) Xiang, S.; Zhang, Y.; Xin, Q.; Li, C. *Angew. Chem., Int. Ed.* **2002**, *41*, 821. (b) Kruk, M.; Jaroniec, M. *Chem. Mater.* **2001**, *13*, 3169. (c) Feng, X.; Fryxell, G. E.; Wang, L. O.; Kim, A. Y.; Liu, J.; Kemner, K. M. *Science* **1997**, *276*, 923. (d) Zhang, L.; Zhang, W.; Shi, J.; Hua, Z.; Li, Y.; Yan, J. *Chem. Commun.* **2003**, 210. (e) Li, G.; Bhosale, S.; Wang, T.; Zhang, Y.; Zhu, H.; Fuhrhop, J.-H. *Angew Chem., Int. Ed.* **2003**, *42*, 3818. (f) Vallet-Regi, M.; Ramila, A.; del Real, R. P.; Perez-Pariente, J. *Chem. Mater.* **2001**, *13*, 308.

(5) For reviews, please see: (a) Moller, K.; Bein, T. *Chem. Mater.* **1998**, *10*, 2950. (b) Bronstein, L. M. *Top. Curr. Chem.* **2003**, *226*, 55. (c) Shi, J.-L.; Hua, Z.-L.; Zhang, L.-X. *J. Mater. Chem.* **2004**, *14*, 795.

(6) (a) Zhang, W.-H.; Shi, J.-L.; Wang, L.-Z.; Yan, D.-S. *Chem. Mater.* **2000**, *12*, 1408. (b) Zhang, W.-H.; Shi, J.-L.; Chen, H.-R.; Hua, Z.-L.; Yan, D.-S. *Chem. Mater.* **2001**, *13*, 648. (c) Zhang, L.-X.; Shi, J.-L.; Yu, J.; Hua, Z.-L.; Zhao, X.-G.; Ruan, M.-L. *Adv. Mater.* **2002**, *14*, 1510. (d) Hua, Z.-L.; Shi, J.-L.; Zhang, L.-X.; Ruan, M.-L.; Yan, J.-N. *Adv. Mater.* **2002**, *14*, 830.(e) Parala, H.; Winkler, H.; Kolbe, M.; Wohlfart, A.; Fischer, R. A.; Schmechel, R.; von Seggern, H. *Adv. Mater.* **2000**, *12*, 1050. (f) Winkler, H.; Birkner, A.; Hagen, V.; Wolf, I.; Schmechel, R.; von Seggern, H.; Fischer, R. A. *Adv. Mater.* **1999**, *11*, 1444.

(7) (a) Brieler, F. J.; Grundmann, P.; Fröba, M.; Chen, L.; Klar, P. J.; Heimbrodt, W.; Nidda, H.-A. K. V.; Kurz, T.; Loidl, A. *J. Am. Chem. Soc.* **2004**, *126*, 797. (b) Coleman, N. R. B.; O'Sullivan, N.; Ryan, K. M.; Crowley, T. A.; Morris, M. A.; Spalding, T. R.; Steytler, D. C.; Holmes, J. D. *J. Am. Chem. Soc.* **2001**, *123*, 7010. (c) Liu, Z.; Sakamoto, Y.; Ohsuna, T.; Hiraga, K.; Terasaki, O.; Ko, C. H.; Shin, H. J.; Ryoo, R. *Angew. Chem., Int. Ed.* **2000**, *39*, 3107. (d) Yang, C.-M.; Sheu, H.-S.; Chao, K.-J. *Adv. Funct. Mater.* **2002**, *12*, 143.

(8) (a) Zhang, W.-H.; Liang, C.; Sun, H.; Xiu, J.; Guan, Y.; Ying, P.; Li. C. *Adv. Mater.* **2002**, *14*, 1776. (b) Ryoo, R.; Joo, S. H.; Kruk, M.; Jaroniec, M. *Adv. Mater.* **2001**, *13*, 677.

10.1021/cm050502h CCC: $30.25
Published on Web 11/16/2005

organic moieties in the structure are covalently linked to each other. Thus, PMOs contain a uniform distribution of organic and inorganic moieties at the molecular level within their frameworks. To date, a series of small mesopore PMOs have been prepared under basic conditions,[11−16] and large pore PMOs have been synthesized under acidic conditions.[17] Bifunctionalized PMOs have also been fabricated by the co-condensation of bridged silsesquioxanes and silicon coupling agents.[18] In particular, Ozin et al.[11] reported the synthesis of methylene-bridged PMOs with a pore size of ~3.1 nm using cetyltrimethylammonium bromide (CTAB) as the structure-directing agent under basic conditions. The methylene groups within the frameworks were stable up to 400 °C, and the ordered structure was retained up to a temperature of 600 °C in air. These robust, thermally stable methylene-bridged PMOs were highlighted as having potential high-temperature applications. Methylene-bridged PMOs with large pores are also highly desirable as hosts for chemical reactions through the selective encapsulation of molecules.[19]

Recent advances in the synthesis of PMOs open up the possibility of exploiting these materials in a range of applications. However, to date there are few reports on the applications of PMOs, and those that have been reported tend to focus on catalysis.[20] Only nanowires of Pt and Pt/Rh alloys,[21] at very low loadings, have been included into PMO templates by wet impregnating and subsequent photoreduction.

To broaden the scope of PMOs and to exploit their potential applications, this work describes the synthesis, surface functionalization, via a supercritical fluid (SCF) grafting reaction, and fabrication of nanostructured semiconductor materials within the channels of large pore methylene-bridged organosilicas (PMO-Me's). Thiol groups were grafted into the frameworks of the PMO-Me materials using an SCF technique, giving rise to bifunctionalized materials (SH-PMO-Me). Subsequent deposition of Au into the pores of SH-PMO-Me allowed them to be used as templates for the incorporation of Ge nanoparticles and nanorods at relatively low temperatures ($360 \leq T \leq 400$ °C). The Ge nanocomposite materials were found to be significantly more crystalline than those formed from Au-coated mesoporous silica templates (SH-SBA-15), highlighting the benefits of using PMOs as hosts for the encapsulation of semiconductor nanomaterials.

Experimental Section

Chemicals. Large pore methylene-bridged periodic mesoporous organosilicas (PMO-Me's) were synthesized using 1,2-bis(triethoxysily)methylene (BTESM) (96%, Gelest) as the organosilica precursor. 3-Mercaptopropyltrimethoxysilane (MPTS) (Aldrich) was used to produce the bifunctionalized PMO (SH-PMO-Me). Pluronic P123 ($EO_{20}PO_{70}EO_{20}$) (BASF) was used as the structural directing agent, and HCl (37% w/v) and NaCl were used as an acid source and additive, respectively. SBA-15 materials were prepared using TEOS and P123. An absolute ethanol/HCl solution was used to remove the surfactant P123 from the PMO templates. $HAuCl_4 \cdot 2H_2O$ was used to synthesize the Au catalyst, and diphenylgermane (DPG) (Gelest) was used to synthesize the Ge nanocrystals. Hexane was used as the SCF medium for the inclusion of Ge nanocrystals within the mesopores. All chemicals were used as received.

Synthesis. PMO-Me was synthesized on the basis of the reported preparation of ethane-bridged PMOs.[17b] Typically, 1.25 g of P123 and 3.5 g of NaCl were dissolved in 40 mL of 0.5 M HCl solution. The solution was stirred at 35−40 °C for more than 5 h, and 2.1 mL of BTESM was added quickly under vigorous stirring for 20 h. The resultant gels were then aged at 80 °C for 60 h statically. The white powders were collected, washed, and dried at 60 °C for at least 20 h in air. The surfactant extraction from the as-synthesized PMO-Me mesophases was carried out two times according to the reported process[18a] using an ethanol/HCl solution, resulting in mesoporous PMO-Me. SBA-15 was synthesized according to the literature using TEOS as a silica source.[22] The surfactant template was removed by calcining at 500 °C for 10 h in air. PMO-Me and SBA-15 were functionalized with thiol groups using an SCF grafting reaction as previously reported.[23] The resultant thiol-functionalized PMO-Me and SBA-15 were named SH-PMO-Me and SH-SBA-15, respectively. Au clusters were synthesized within the channels of SH-PMO-Me and SH-SBA-15 channels as previously reported.[24] The Au clusters in the pores of SH-PMO-Me and SH-SBA-15 were

(9) (a) Chen, H.-R.; Shi, J.-L.; Li, Y.-S.; Yan, J.-N.; Hua, Z.-L.; Chen, H.-G.; Yan, D.-S. *Adv. Mater.* **2003**, *15*, 1078. (b) Vettraino, M.; Ye, ; He, X.; Antonelli, D. M. *Aust. J. Chem.* **2001**, *54*, 85.
(10) (a) Stein, A.; Melde, B. J.; Schroden, R. C. *Adv. Mater.* **2000**, *12*, 1403. (b) Sayari, A.; Hamoudi, S. *Chem. Mater.* **2001**, *13*, 3151. (c) Kickelbick, G. *Angew. Chem., Int. Ed.* **2004**, *43*, 3102.
(11) Asefa, T.; MacLachlan, M. J.; Grondey, H.; Coombs, N.; Ozin, G. A. *Angew. Chem., Int. Ed.* **2000**, *39*, 1808.
(12) Inagaki, S.; Guan, S.; Fukushima, Y.; Ohsuna, T.; Terasaki, O. *J. Am. Chem. Soc.* **1999**, *121*, 9611.
(13) (a) Asefa, T.; MacLachan, M. J.; Coombs, N.; Ozin, G. A. *Nature* **1999**, *402*, 867. (b) Melde, B. J.; Holland, B. T.; Blanford, C. F.; Stein, A. *Chem. Mater.* **1999**, *11*, 3302.
(14) Inagaki, S.; Guan, S.; Ohsuna, T.; Terasaki, O. *Nature* **2002**, *416*, 304.
(15) (a) Kapoor, M. P.; Yang, Q.; Inagaki, S. *J. Am. Chem. Soc.* **2002**, *124*, 15176. (b) Kapoor, M. P.; Yang, Q.; Inagaki, S. *Chem. Mater.* **2004**, *16*, 1209.
(16) Yoshina-Ishii, C.; Asefa, T.; Coombs, N.; MacLachlan, M. J.; Ozin, G. A. *Chem. Commun.* **1999**, 2539.
(17) (a) Matos, J. R.; Kruk, M.; Mercuri, L. P.; Jaroniec, M.; Asefa, T.; Coombs, N.; Ozin, G. A.; Kamiyama, T.; Terasaki, O. *Chem. Mater.* **2002**, *14*, 1903. (b) Guo, W.; Park, J.-Y.; Oh, M.-O.; Jeong, H.-W.; Cho, W.-J.; Kim, I.; Ha, C.-S. *Chem. Mater.* **2003**, *15*, 2295. (c) Wang, W.; Xie, S.; Zhou, W.; Sayari, A. *Chem. Mater.* **2004**, *16*, 1756. (d) Bao, X. Y.; Zhao, X. S.; Li, X.; Chia, P. A.; Li, J. *J. Phys. Chem. B* **2004**, *108*, 4684.(e) Guo, W.; Kim, I.; Ha, C. S. *Chem. Commun.* **2003**, 2692.
(18) (a) Zhu, H.; Jones, D. J.; Zajac, J.; Dutartre, R.; Rhomari, M.; Rozière, J. *Chem. Mater.* **2002**, *14*, 4886. (b) Yang, Q.; Kapoor, M. P.; Inagaki, S. *J. Am. Chem. Soc.* **2002**, *124*, 9694. (c) Asefa, T.; Kruk, M.; MacLachlan, M. J.; Coombs, N.; Grondey, H.; Jaroniec, M.; Ozin, G. A. *J. Am. Chem. Soc.* **2001**, *123*, 8520. (d) Burleigh, M. C.; Dai, S.; Hagaman, E. W.; Lin, J. S. *Chem. Mater.* **2001**, *13*, 2537. (e) Burleigh, M. C.; Markowitz, M. A.; Spector, M. S.; Gaber, B. P. *Chem. Mater.* **2001**, *13*, 4760. (f) Burleigh, M. C.; Markowitz, M. A.; Spector, M. S.; Gaber, B. P. *J. Phys. Chem. B* **2001**, *105*, 9935.
(19) (a) Rao, M. S.; Dave, B. C. *J. Am. Chem. Soc.* **1998**, *120*, 13270. (b) Han, Y.-J.; Stucky, G. D.; Butler, A. *J. Am. Chem. Soc.* **1999**, *121*, 9897.
(20) (a) Kapoor, M. P.; Sinha, A. K.; Seelan, S.; Inagaki, S.; Tsubota, S.; Yoshida, H.; Haruta, M. *Chem. Commun.* **2002**, 2902. (b) Bhaumik, A.; Kapoor, M. P.; Inagaki, S. *Chem. Commun.* **2003**, 470. (c) Yuan, X.; Lee, H. I.; Kim, J. W.; Yie, J. E.; Kim, J. M. *Chem. Lett.* **2003**, *32*, 650. (d) Kapoor, M. P.; Bhaumik, A.; Inagaki, S.; Kuraoka, K.; Yazawa, T. *J. Mater. Chem.* **2002**, *12*, 3078.
(21) (a) Fukuoka, A.; Sakamoto, Y.; Guan, S.; Inagaki, S.; Sugimoto, N.; Fukushima, Y.; Hirahara, K.; Iijima, S.; Ichikawa, M. *J. Am. Chem. Soc.* **2001**, *123*, 3373. (b) Sakamoto, Y.; Fukuoka, A.; Higuchi, T.; Shimomura, N.; Inagaki, S.; Ichikawa, M. *J. Phys. Chem. B* **2004**, *108*, 853.
(22) Zhang, W.-H.; Lu, J.; Han, B.; Li, M.; Xiu, J.; Ying, P.; Li, C. *Chem. Mater.* **2002**, *14*, 3413.
(23) Zhang, W.-H.; Lu, X.-B.; Xiu, J.-H.; Hua, Z.-L.; Zhang, L.-X.; Robertson, M.; Shi, J.-L.; Yan, D.-S.; Holmes, J. D. *Adv. Funct. Mater.* **2004**, *14*, 544.

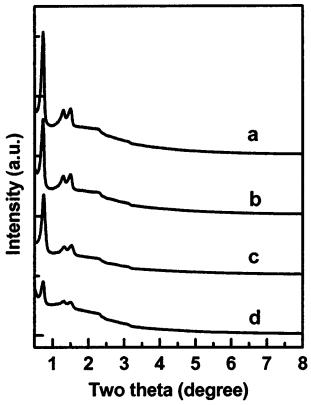

Figure 1. XRD patterns of PMO-Me samples synthesized at different acid concentrations: (a) PMO-Me(1.0 M), (b) PMO-Me(0.5 M), (c) PMO-Me(0.2 M), and (d) PMO-Me(0.1 M).

subsequently used as catalysts for the growth of Ge nanocrystals within the pores. Ge nanocrystals were synthesized in supercritical hexane at a pressure of 300 atm and at temperatures of 360, 380, and 400 °C for 1 h. The products were correspondingly designated as Ge-SH-PMO-Me(360), Ge-SH-PMO-Me(380), and Ge-SH-PMO-Me(400), respectively. For comparison purpose, Ge nanocrystals were also grown inside the channels of thiol-functionalized mesoporous silica, resulting in Ge-SH-SBA-15, using the Au clusters as catalysts in supercritical hexane at a pressure of 300 atm and a temperature of 380 °C for 1 h.

Characterization. X-ray diffraction (XRD) data were collected on a Philips PW3710 MPD powder diffractometer, using Cu Kα radiation, operated at 40 kV and 40 mA. Scanning electron microscopy (SEM) was performed on a JEOL 5500 system at a beam energy of 25 kV. Transmission electron microscopy (TEM), electron diffraction (ED), and energy dispersive spectroscopy (EDS) analyses were carried out on a JEOL 200 CX electron microscope operating at 200 kV. N_2 sorption isotherms were obtained on a Micrometrics Gemini III 2375 analyzer. The samples were degassed at 200 °C under nitrogen for 20 h before measurement. The pore size distributions (PSDs) were calculated using the Barret−Joyner−Halenda (BJH) method based on the adsorption branches of the sorption isotherms, and the pore sizes were estimated from the position of the maximum in the PSDs. Both solid state ^{29}Si magic angle spinning (MAS) NMR and ^{13}C cross polarization (CP) MAS NMR were collected on a Bruker DRX-400 NMR spectrometer. The ^{29}Si MAS NMR spectra were recorded in a 4 mm ZrO_2 rotor at 79.4 MHz, with a pulse width of 3.0 μs, MAS rate of 4 kHz, and acquisition time of 40.96 ms. The ^{13}C CP MAS NMR spectra were measured at 100.5 MHz, with a pulse time of 5.6 μs, MAS rate of 4 kHz, and acquisition time of 25.60 ms. Quantitative analyses were performed to explain the NMR spectra.

Results and Discussion

Synthesis of PMO-Me. A series of PMO-Me samples were prepared at acid concentrations of 1.0, 0.5, 0.2, and 0.1 M. Figure 1 displays the X-ray diffraction (XRD) patterns of the samples prepared, designated as PMO-Me(x M) (x = 1.0, 0.5, 0.2, and 0.1) after removal of the surfactant template. All the samples displayed four diffraction peaks, (100), (110), (200), and (210), indicating that highly ordered PMOs with SBA-15-type structures were synthesized.[3a] The intensity of the diffraction peaks was also observed to increase with

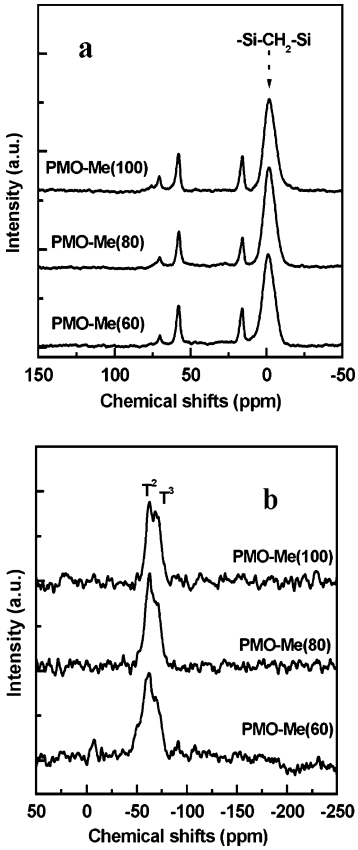

Figure 2. (a) Solid state ^{13}C CP MAS NMR and (b) ^{29}Si MAS NMR for the PMO-Me samples synthesized at different temperatures.

increasing acid concentrations. Hence, highly acidic conditions are beneficial for the formation of well ordered PMO-Me. However, an attempt to prepare PMO-Me from a 1.5 M HCl solution resulted in a gel-like product which could not be separated from the mother liquid. It was also difficult to separate the PMO-Me sample synthesized at an acid concentration of 1.0 M from solution. Consequently, PMO-Me samples produced at acid concentrations of 0.5 M PMO-Me(0.5 M) were chosen for further investigation.

All PMO samples prepared to date, and reported in the literature, in strongly acidic conditions have been undertaken at temperatures below 80 °C to avoid the possible cleavage of Si−C bonds within the frameworks. To understand this problem, three PMO-Me samples, PMO-Me(100), PMO-Me(80), and PMO-Me(60), were prepared by aging the gels at 100, 80, and 60 °C respectively (note: PMO-Me(0.5 M) and PMO-Me(80) is the same sample). The XRD patterns of the PMO-Me samples produced at different aging temperatures (Supporting Information Figure S1) show that highly ordered PMO materials are obtained at each temperature. Figure 2a shows the ^{13}C CP MAS NMR spectra for the PMO-Me samples prepared at varying aging temperatures. A strong signal at −1.5 ppm, assigned to the carbons in the Si−CH_2−Si groups, was observed with all of the samples analyzed. This result confirms the presence of the methylene groups inside the frameworks of PMO-Me.[11,25] The small signal at 70.5 ppm arises from the ethylene oxide

(24) Guari, Y.; Thieuleux, C.; Mehdi, A.; Reyé, C.; Corriu, R. J. P.; Gomez-Gallardo, S.; Philippot, K.; Chaudret, B. *Chem. Mater.* **2003**, *15*, 2017.

(25) Zhou, Z.; Bao, X.; Zhao, X. S. *Chem. Commun.* **2004**, 1376.

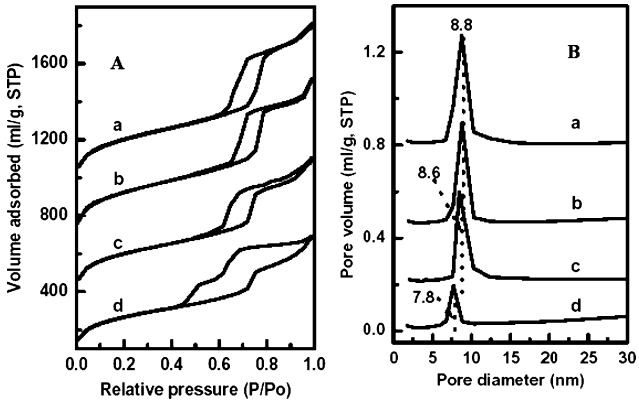

Figure 3. (A) N_2 sorption isotherms and(B) pore size distributions (PSDs) of (a) PMO-Me (1.0 M), (b) PMO-Me (0.5 M), (c) PMO-Me (0.2 M), and (d) PMO-Me (0.1 M).

block of the P123 surfactant.[26] The peak at 57.9 ppm is attributed to the carbons from the surface ethoxy groups (Si-OCH_2CH_3), which form during solvent extraction in acidic ethanol solutions.[27] Both the methyl groups in the propylene oxide block of the P123[26] and the Si-OCH_2CH_3 groups on the surfaces[27] could possibly be responsible for the resonance at 15.9 ppm. These results show that a small amount of P123 was still present in our samples after the extraction process. The ^{29}Si MAS NMR shown in Figure 2b gives two strong signals at −62.7, and −69.4 ppm, corresponding to partially condensed T^2 Si[RSi(OSi)$_2$(OH)] and fully condensed T^3 Si[RSi(OSi)$_3$] resonances.[28] The intensity of the T^3 silicon tends to increase with increasing aging temperatures, suggesting that a higher temperature is beneficial to the condensation of the frameworks of PMO-Me. The absence of the signals of Q^n Si[Si(OSi)$_n$(OH)$_{4-n}$] species between −90 to −120 ppm indicates that all silicon atoms are covalently connected to carbon atoms and no Si−C bond cleavage has occurred under the strongly acidic conditions, even for the hydrothermally treated sample PMO-Me(100). These results demonstrate that the Si−CH_2−Si bonds have a high hydrothermal stability. The large intensity of the T^2 signal is also indicative of the incomplete condensation of the organosilane precursor; namely, a large number of free silanol groups are still present in the framework of the PMO-Me. This result is important as these silanol groups can act as active sites to anchor functional groups, via a grafting reaction,[23,29] allowing surface modification of PMOs by a postsynthesis method.

N_2 adsorption isotherms for the PMO-Me samples prepared at different acid concentrations in Figure 3a are all type IV classifications,[30] displaying sharp capillary condensation at relative pressures of 0.6−0.8. The hysteresis loops, with parallel and nearly vertical branches in all of the isotherms except for PMO-Me (0.1 M), are type H1 hysteresis, according to IUPAC definitions, which is characteristic of materials with a high degree of pore size uniformity.[31−33] In contrast, the PMO-Me (0.1 M) material showed a complex N_2 sorption isotherm. The one-step capillary condensation in the range $0.7 \leq P/P_0 \leq 0.8$, which occurs inside the ordered pores, in the adsorption branch and the two-step evaporation in the range $0.46 \leq P/P_0 \leq 0.7$ in the desorption branch are indicative of uniform mesopores with windows caused by pore blocking.[34] The hysteresis loop at high relative pressures ($P/P_0 \geq 0.8$) could be attributed to the pore blocking effects,[34] or the secondary pores running across the framework of mesoporous materials,[33] or even impurities formed from the liquid-crystal templating process.[35] The pore size distributions (PSDs) for the PMO-Me samples in Figure 3b present narrow and sharp peaks, indicating high-quality samples. The N_2 sorption properties (sorption isotherms and pore size distributions) for the PMO-Me samples prepared at different temperatures (Supporting Information Figure S2) show that they are high quality mesoporous materials. Table 1 lists the structural parameters for all of the PMO-Me samples investigated in this study. The pore diameters of the PMO-Me samples increased with rising solution acidity to a certain degree, but no clear explanation for this result can be provided at present. In short, our experiments show that high-quality PMO-Me with large pores can be prepared using P123 as templates under strong acidic conditions (0.2 M ≤ HCl concentration ≤ 1.0 M).

Table 1. Structural Parameters for PMO-Me Samples Synthesized under Different Conditions

	d_{100} (nm)	BET surface area (m^2/g)	pore diameter (nm)	pore volume (mL/g)
PMO-Me(1.0 M)	12.00	1047.8	8.8	0.971
PMO-Me(0.5 M)[a]	12.00	1125.5	8.8	0.999
PMO-Me(0.2 M)	11.78	1033.6	8.6	0.926
PMO-Me(0.1 M)	11.79	915.4	7.8	0.758
PMO-Me(60)	11.77	1017.6	7.8	0.819
PMO-Me(100)	12.00	1030.6	8.8	0.984

[a] PMO-Me(80) = PMO-Me (0.5 M).

Ordered mesoporous silicas prepared using P123 tend to form rodlike structures, but other morphologies can also be obtained if certain additives are added during synthesis.[36] PMO-Me(1.0 M) showed no defined morphology at low-magnification by SEM, but at high magnification small particles with diameters less than 1 μm (Figure 4a,b) were observed. PMO-Me(0.5 M) samples demonstrated rodlike structures of poorly defined shapes (Figure 4c). High-resolution SEM demonstrated that the rodlike structures were aggregates (or architectures) of many small particles and rods with diameter less than 1 μm (Figure 4d). In contrast, PMO-

(26) Yang, C.-M.; Zibrowius, B.; Schmidt, W.; Schüth, F. *Chem. Mater.* **2003**, *15*, 3739.
(27) Guan, S.; Inagaki, S.; Ohsuna, T.; Terasaki, O. *Microporous Mesoporous Mater.* **2001**, *44*−*45*, 165.
(28) Sayari, A.; Hamoudi, S.; Yang, Y.; Moudrakovski, I. L.; Ripmeester, J. R. *Chem. Mater.* **2000**, *12*, 3857.
(29) Zhao, X. S.; Lu, G. Q.; Whittaker, A. K.; Millar, G. J.; Zhu, H. Y. *J. Phys. Chem. B* **1997**, *101*, 6525.
(30) Sing, K. S. W.; Everett, D. H.; Haul, R. A. W.; Moscou, L.; Pierotti, R. A.; Rouquerol, J.; Siemieniewska, T. *Pure Appl. Chem.* **1985**, *57*, 603.
(31) Kruk, M.; Jaroniec, M. *Chem. Mater.* **2001**, *13*, 3169.
(32) Kruk, M.; Jaroniec, M.; Sayari, A. *Langmuir* **1997**, *13*, 6267.
(33) Kruk, M.; Jaroniec, M.; Sakamoto, Y.; Terasaki, O.; Ryoo, R.; Ko, C. H. *J. Phys. Chem. B* **2000**, *104*, 292.
(34) (a) Van Der Voort, P.; Ravikovitch, P. I.; De Jong, K. P.; Benjelloun, M.; Van Bavel, E.; Janssen, A. H.; Neimark, A. V.; Weckhuysen, B. M.; Vansant, E. F. *J. Phys. Chem. B* **2002**, *106*, 5873. (b) Kruk, M.; Jaroniec, M.; Joo, S. H.; Ryoo, R. *J. Phys. Chem. B* **2003**, *107*, 2205.
(35) Huo, Q.; Leon, R.; Petroff, P. M.; Stucky, G. D. *Science* **1995**, *268*, 1324.
(36) (a) Schmidt-Winkel, P.; Yang, P.; Margolese, D. I.; Chmelka, B. F.; Stucky, G. D. *Adv. Mater.* **1999**, *11*, 303. (b) Zhao, D.; Sun, J.; Li, Q.; Stucky, G. D. *Chem. Mater.* **2000**, *12*, 275. (c) Kosuge, K.; Sato, T.; Kikukawa, N.; Takemori, M. *Chem. Mater.* **2004**, *16*, 899.

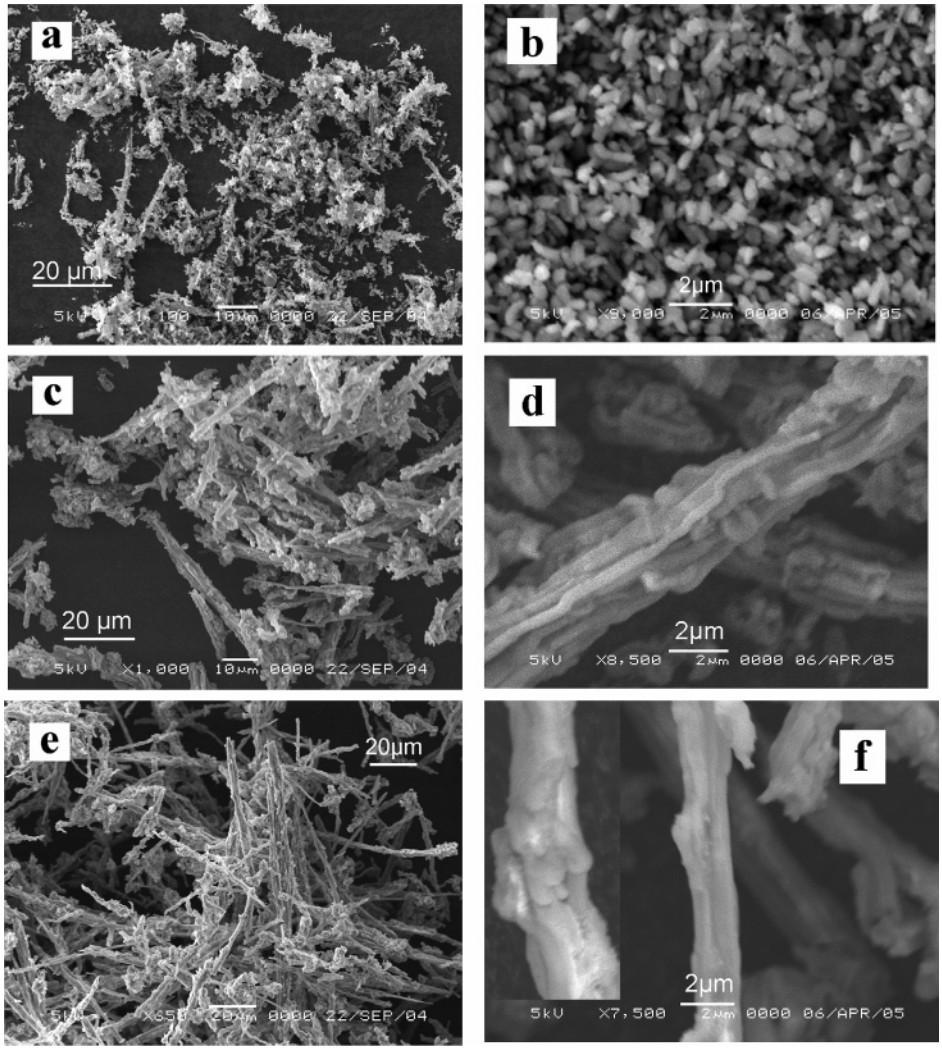

Figure 4. SEM images of PMO-Me samples synthesized at different conditions: (a) and (b) PMO-Me (1.0 M), (c) and (d) PMO-Me (0.5 M) and (e) and (f) PMO-Me (0.2 M).

Me(0.2 M) samples were observed to be well-defined rods (Figure 4e,f). Thus, the morphology of the PMO-Me produced is highly dependent on the solution acidity. The morphology of the mesophases is possibly controlled by the kinetic balance between the hydrolysis rate of the organosilica precursor, BTESM, and the rate of assembly of the P123 surfactant and the organosilicates (resulting from the hydrolysis of the BTESM). The fast hydrolysis rate of BTESM in high acidic solution, e.g., 1.0 M HCl, possibly results in the formation of many mesophase nucleates which are detrimental to the subsequent growth of these aggregates into larger morphologies. In contrast, at lower acidic condition, e.g., in a 0.2 M HCl solution, the hydrolysis rate of BTESM is lower and closer to the rate of assembly of P123 and the organosilicates. Hence, the amount of mesophase nucleates produced is relatively small, compared to the highly acidic conditions, allowing gradual growth of the resulting materials into a regular morphology.

Bifunctionalization of PMO-Me via Postsynthesis. Two approaches, namely, direct synthesis and postsynthesis (grafting), are widely used to functionalize ordered mesoporous silicas.[23] As discussed above, it is possible to modify the surfaces of PMO-Me materials by postsynthesis due to the presence of free silanol groups (T^2 Si atoms). In our experiments, grafting of PMO-Me materials was undertaken in an SCF medium, due to the efficiency of this method to anchor functional groups onto the pore walls of OMMs compared to traditional protocols, e.g., using toluene as the solvent in a conventional reflux process.[23] Small-angle XRD patterns of the PMO-Me(80) and SH-PMO-Me samples (Supporting Information Figure S3) demonstrate that both samples are highly ordered mesoporous materials. ^{29}Si MAS NMR and ^{13}C CP MAS NMR spectroscopy were used to check the attachment of the thiol groups onto the pore walls of PMO-Me(80) via the SCF grafting reaction. The decrease in the signal intensity of the T^2 Si atoms (with one free silanol group) or increase in T^3 Si atoms (no free silanol group) provides direct evidence for anchoring of the functional groups. Figure 5a depicts the ^{29}Si MAS NMR spectra for the PMO-Me(80) and the SH-PMO-Me samples. The T^3 intensity was largely enhanced after the grafting reaction, and the ^{13}C CP MAS NMR spectra for the SH-PMO-Me materials (Figure 5b) show two additional signals located at 11.3 and 26.6 ppm compared to those of the PMO-Me(80) samples. The former signal is ascribed to the methylene carbon group directly bonded to the silicon atom (C1), and the latter signal to the other two methylene carbon groups [C2 and C3 in $Si-CH_2(1)CH_2(2)CH_2(3)SH$].[18b,37] These

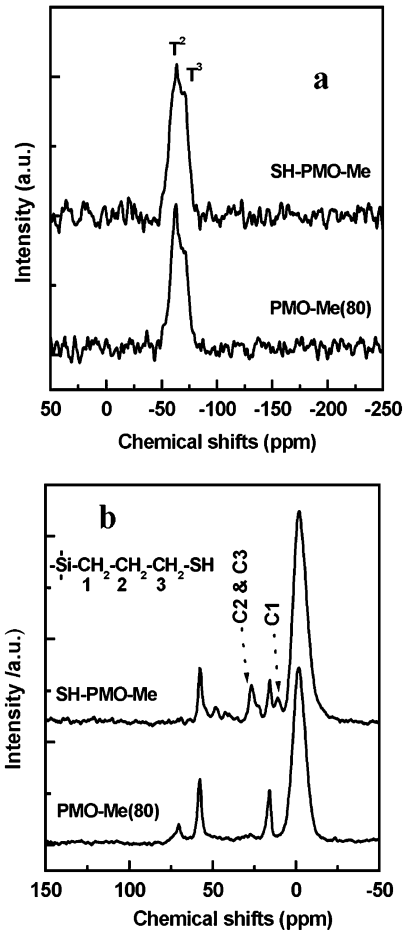

Figure 5. (a) Solid state ^{29}Si MAS NMR and (b) ^{13}C CP MAS NMR spectra for PMO-Me(80) and SH−PMO-Me.

results demonstrate that PMO-Me(80) has been successfully functionalized by thiol groups via SCF grafting methods, resulting in the formation of bifunctionalized SH-PMO-Me materials. The decrease in the band intensity of the surface ethoxy groups, Si−OCH_2CH_3 at 57.9 and 15.9 ppm, shows that the T^3 Si can also be anchored with functional groups, i.e., by replacing the ethoxy groups with MPTS in the present experiment. In addition, the disappearance of the NMR band at 70.5 ppm for the SH-PMO-Me sample highlights that the functionalization process in the SCF medium can further remove the P123 from the parent mesophase. Figure 6 shows the N_2 sorption isotherms and pore size distributions for the samples PMO-Me(80) and SH−PMO-Me. After grafting, the BET surface areas, pore diameters, and pore volumes decreased from 1125.5 m^2/g, 8.8 nm, and 0.999 mL/g for PMO-Me(80) to 992.1 m^2/g, 8.0 nm, and 0.898 mL/g for SH-PMO-Me, providing further evidence that PMO-Me(80) has been efficiently functionalized via postsynthesis. Chemical analysis showed that the S content in the SH-PMO-Me samples was 2.6 wt % and 3.4 wt % in the SH-SBA-15 samples prepared by the same SCF process. Thus, the surface silanol groups in the channels of SB-15 available for grafting were estimated to be approximately 1.3 times greater than in the PMO-Me samples. Attempts to anchor MPTS onto

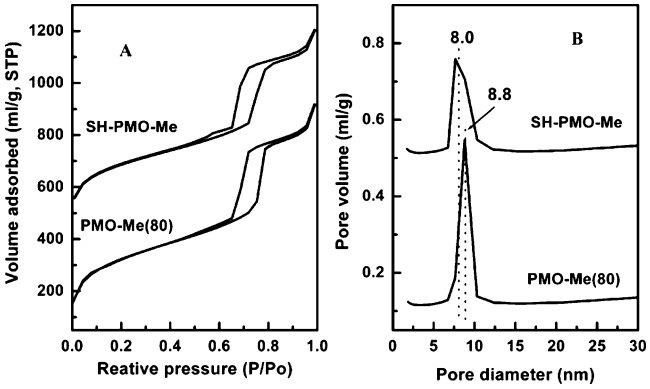

Figure 6. (A) N_2 sorption isotherms and (B) pore size distributions (PSDs) for PMO-Me(80) and SH-PMO-Me.

the pore walls of PMO-Me samples using toluene as a solvent and refluxing gave rise to rather disappointing results, a maximum S loading of 0.5 wt % was obtained.[38] Therefore, the SCF approach is highly efficient at functionalizing PMO-Me materials compared to traditional protocols. The high diffusivity and negligible surface tension of the SCF allow efficient transport and distribution of the target molecule, in this case MPTS, into the mesopores of PMO-Me samples, compared to traditional protocols.

Synthesis of Ge Nanocrystals within SH-PMO-Me Materials. Previously, we have reported the synthesis of nanocrystals, such as Si,[7b] Ge,[39] and Fe_3O_4,[40] inside the channels of mesoporous silicas using SCF inclusion techniques. Ge nanowires can be produced inside mesoporous silica templates by decomposing diphenylgermane (DPG), or diethyl germane, in an SCF at high temperatures and pressures, typically 500 °C and 375 bar, respectively. However, this high-temperature approach is not suitable for the inclusion of Ge nanocrystals in the channels of SH-PMO-Me materials due to its relatively low thermal stability compared to mesoporous silica. We have therefore developed a low-temperature approach ($360 \leq T \leq 400$ °C) to grow Ge nanocrystals within SH-PMO-Me templates using Au clusters, formed within the mesopores,[24] as a catalyst. As a comparison, Ge nanocrystals were also prepared inside Au-containing SH-SBA-15 samples under identical conditions.

Figure 7 shows the small-angle XRD patterns from a Ge-containing SH-PMO-Me sample and a SH-PMO-Me material without Ge. All the diffraction peaks, with significantly reduced intensity, can be observed after the Ge inclusion within the pores, indicative of retaining highly ordered structures for the Ge-SH-PMO-Me samples. The decrease in the XRD peak intensity has been well-documented for mesoporous nanocomposites.[41,42] In the ordered mesoporous samples, the intensity of the Bragg reflection originates from the difference in the scattering power between the frame-

(37) (a) Liu, A. M.; Hidajat, K.; Kawi, S.; Zhao, D. Y. *Chem. Commun.* **2000**, 1145. (b) Wang, L.-Q.; Liu, J.; Exarhos, G. J.; Bunker, B. C. *Langmuir* **1996**, *12*, 2663.

(38) Our experiment to reflux the mixture of PMO-Me and MPTS in toluene for 8 h resulted in no pore size changes by N_2 sorption measurement. A similar study showed that the surface silanol of the PMOs available for the silicon coupling agent amounted to ~5% of the mesoporous silica. Please see: Chung, J.-S.; Kim, D.-J.; Ahn, W.-S.; Ko, J.-H.; Cheong, W.-J. *Korean J. Chem. Eng.* **2004**, *21*, 132.

(39) Coleman, N. R. B.; Ryan, K. M.; Spalding, T. R.; Holmes, J. D.; Morris, M. A. *Chem. Phys. Lett.* **2001**, *343*, 1.

(40) Crowley, T. A.; Ziegler, K. J.; Lyons, D. M.; Erts, D.; Olin, H.; Morris, M. A.; Holmes, J. D. *Chem. Mater.* **2003**, *15*, 3518.

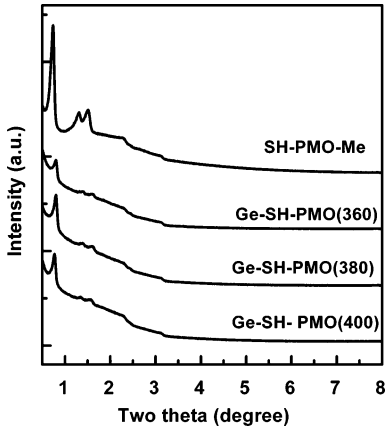

Figure 7. Small-angle XRD patterns of SH-PMO-Me and Ge-containing PMO-Me samples.

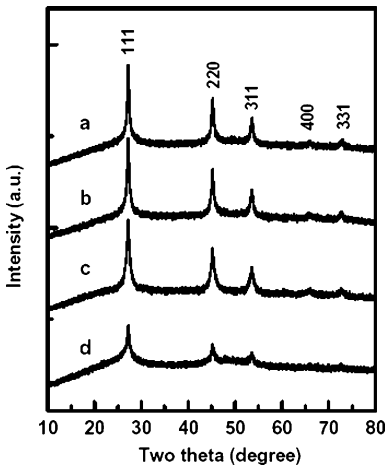

Figure 8. Wide-angle XRD patterns of (a) Ge-SH-PMO-Me(360), (b) Ge-SH-PMO-Me(380), (c) Ge-SH-PMO-Me(400), and (d) Ge-SH-SBA-15.

works and the empty pores. Upon encapsulation of the pores with Ge, the scattering power within the pores is enhanced, resulting in a loss in the scattering contrast with the template framework and a reduction in the XRD intensities.[41]

Figure 8 displays the wide-angle XRD patterns for the Ge-SH-PMO-Me and Ge-loaded mesoporous silica (Ge-SH-SBA-15) samples. Five peaks can be readily attributed to (111), (220), (311), (400), and (331) lattice planes of Ge with a diamond structure for the Ge-SH-PMO nanocomposite materials. In contrast, only three strong peaks, (111), (220), and (311), are well-resolved for the Ge-SH-SBA-15 materials (trace d), and the peak intensities of the Ge-SH-PMO-Me samples are stronger than those from Ge-SH-SBA-15. These results possibly suggest that SH-PMO-Me is a better host than mesoporous silica for the formation of highly crystalline Ge nanocystals in the present experiments. This result could be attributed to the greater hydrophobic nature of the mesochannels within SH-PMO-Me compared to SH-SBA-15.[13b,43] Hence, it is easier for the organogermane (DPG) to diffuse into and react with the Au clusters in the channels

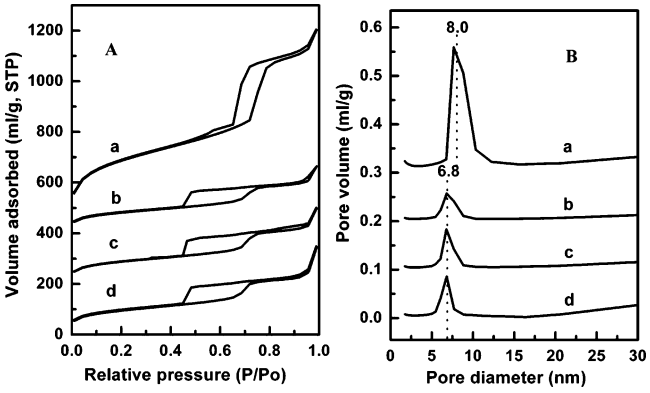

Figure 9. (A) N_2 sorption isotherms and pore size distributions (B) of (a) SH-PMO-Me, (b) Ge-SH-PMO-Me(360), (c) Ge-PMO-Me(380), and (d) Ge−PMO-Me(400).

Table 2. Structural Parameters of Ge−SH−PMO-Me Samples and Their Host Template (SH-PMO-Me)

	d_{100} (nm)	BET surface area (m^2/g)	pore diameter (nm)	pore volume (mL/g)
SH-PMO-Me	11.90	992.1	8.0	0.898
Ge-SH-PMO(360)	11.35	285.5	6.8	0.252
Ge-SH-PMO(380)	10.98	307.0	6.8	0.284
Ge-SH-PMO(400)	10.96	329.6	6.8	0.293

of SH-PMO-Me, compared to SH-SBA-15, resulting in highly crystalline Ge nanocrystals within the pores. In the absence of a Au catalyst, high temperatures, typically 500 °C, are required to produce crystalline Ge inside the channels of mesoporous silica,[39] indicating the importance of the catalyst in the formation of highly crystalline Ge nanomaterials at low temperatures in the present experiment. Therefore, our experiments present a catalytic strategy for growing highly crystalline nanomaterials within the pores of ordered mesoporous materials at relatively low temperatures.

Figure 9 displays N_2 sorption isotherms and pore size distributions (PSDs) for the Ge-SH-PMO-Me and SH-PMO-Me samples, and Table 2 presents their N_2 sorption properties. The hysteresis loops in the isotherms of the Ge-SH-PMO-Me samples are dramatically delayed to lower relative pressures compared to those of the SH-PMO-Me samples, suggesting that the pores in Ge-SH-PMO-Me are possibly partially blocked. On the other hand, the mesopores are still accessible by N_2 after the formation of Ge nanocrystals, implying that the pores are indeed partially filled by Ge.[31] The BET surface areas, BJH adsorption pore diameters, and pore volumes decreased simultaneously and significantly after the formation of Ge within the mesopores. These results demonstrate that Ge nanocrystals have been formed inside the channels of the SH-PMO-Me templates. Although the pore radii are all centered at 6.8 nm, for the three Ge-SH-PMO-Me samples, the BET surface areas and pore volumes show delicate differences. The BET surface areas increased from 285.5 to 307.0 m^2/g, then to 329.6 m^2/g when the reaction temperatures were increased from 360 to 380 °C, and then to 400 °C, respectively. On the other hand, the pore volumes were enlarged monotonically from 0.258 to 0.284 mL/g, and to 0.293 mL/g with increasing reaction temperatures. These results suggest that a lower temperature is beneficial for the formation of Ge within the channels of

(41) (a) Brieler, F. J.; Fröba, M.; Chen, L.; Klar, P. J.; Heimbrodt, W.; von Nidda, H.-A. K.; Loidl, A. *Chem. Eur. J.* **2002**, *8*, 185. (b) Hammond, W.; Prouzet, E.; Mahanti, S. D.; Pinnavaia, T. J. *Microporous Mesoporous Mater.* **1999**, *27*, 19.
(42) (a) Marler, B.; Oberhagemann, U.; Vortmann, S.; Gies, H. *Microporous Mater.* **1996**, *6*, 375. (b) Lim, M. H.; Blanford, C. F.; Stein, A. *Chem. Mater.* **1998**, *18*, 467.
(43) Zhao, X. S.; Lu, G. Q. *J. Phys. Chem. B* **1998**, *102*, 1556.

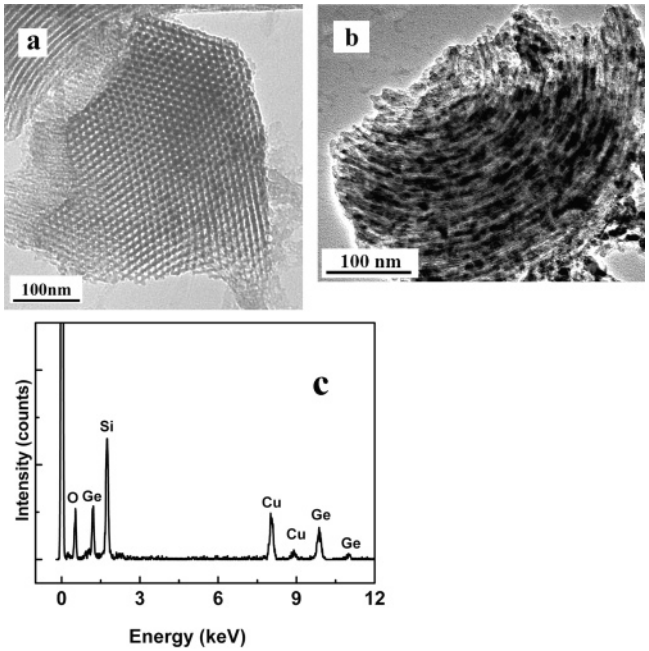

Figure 10. TEM images of (a) PMO-Me(80) and (b) Ge-SH-PMO-Me-(380), and (c) EDS of Ge-SH-PMO-Me(380).

SH-PMO-Me. Korgel et al.[44] have studied the growth kinetics of Ge nanowires seeded by Au clusters in SCF media. The optimized reaction temperature was found to be between 350 and 450 °C. At higher temperature, such as 500 °C, the DPG decomposed too quickly and a large portion of the Ge atoms produced were homogeneously nucleated into spherical particles rather than wires. However, at lower temperatures, such as 300 °C, DPG decomposition occurred too slowly, and the limited Ge atoms produced did not meet the growth rate required to form nanowires.

A TEM image of the PMO-Me(80) sample (Figure 10a), before nanowire inclusion, clearly shows the highly ordered hexagonal structure of the sample.[3a] Figure 10b shows a TEM image of PMO-Me(80) after Ge formation within the mesochannels at a reaction temperature of 380 °C (Ge-SH-PMO-Me(380)). Both Ge nanoparticles and short nanowires (black images) can be observed along the channels of the mesoporous host. Energy dispersive spectrum (EDS) analysis on the area shown in Figure 10b is displayed in Figure 10c. Strong Ge and Si signals with atomic ratios of Ge/Si of 29.6% were obtained, much higher than the loading of Pt within PMOs as previously reported, with atomic ratios of Pt/Si less than 2% (5 wt %).[21] To harvest the free-standing Ge nanomaterials in this study, the frameworks of the Ge−SH−PMO-Me(380) sample were removed using a dilute HF/ethanol solution[21b] resulting in the formation of self-supported Ge nanostructures. The TEM image provided in Figure 11a shows the presence of free-standing Ge nanoparticles and nanorods with diameters between 5 and 7 nm and lengths up to 30 nm, which are consistent with mesochannel dimensions of SH-PMO-Me. The corresponding high-resolution TEM (HRTEM) images (Figure 11b) present the well-resolved lattice fringes of the Ge nanorods, and the electron diffraction (ED) patterns, depicted in Figure 11c, suggest that the Ge nanostructures are polycrystalline in nature. EDS analysis (Figure 11d) confirmed the removal of the frameworks of the SH-PMO-Me template by HF/ethanol and that the nanocrystals are indeed composed of Ge. For comparison purpose, free-standing Ge nanocrystals were also obtained by removing the frameworks from the Ge-SH-SBA-15 samples with an HF solution. The resultant Ge nanomaterials mainly consisted of nanoparticles, and Ge nanorods were seldom found by TEM. Typical TEM images of the free-standing Ge nanocrystals templated by SH-SBA-15 are depicted in Figure 11e (low-magnification TEM images) and in Figure 11f (high-resolution TEM images). The diameter of Ge nanoparticles formed within SH-SBA-15 was found to have a broader distribution, compared to that of SH-PMO-Me, of between 5 and 12 nm. Within the SH-PMO-Me materials, Ge nanocrystals are seeded by Au clusters, and their diameters are limited by the pore dimensions of the templates. At low temperatures, the rate at which DPG is transported into mesopores matches the rate at which DPG decomposes resulting in the formation of both nanoparticles and nanorods. The greater hydrophilic nature of SH-SBA-15 pores compared to SH-PMO-Me results in a lower rate of diffusion of DPG into the mesochannels and hence the greater tendency to form nanoparticles at lower loadings. The formation of highly crystalline Ge nanorods could further be explained by a supercritical fluid−liquid−solid (SCF-L-S) process, which a modification of the well-known vapor−liquid−solid (VLS) mechanism commonly used for growing of one-dimensional materials.[45] The eutectic temperature of Au/Ge is 360 °C, and the Au clusters and Ge initially form liquid drops at temperature higher than the eutectic temperature. These liquid drops act as nucleates to direct the growth of Ge nanowires if sufficient Ge precursor can be supplied.[46] In our case, the formation of Ge nanomaterials inside the mesopores was limited by the amount of Au clusters in the pores and also by the diffusion of the Ge precursor into the channels of PMO-Me; therefore, a significant mix of both nanorods and nanoparticles was obtained.

Additionally, Si nanomaterials have also been prepared using PMO-Me and SBA-15 as templates at 400 °C by the catalytic SCF approach mentioned. XRD data from these samples again demonstrate that PMOs are advantageous over mesoporous silicas as templates for the formation of nanoscale Si materials with higher crystalline structures (Supporting Information Figure S4). The resultant Si nanomaterials formed within the PMO-Me templates have a much higher crystallinity than those formed within mesoporous silica templates at 500 °C by an SCF process without a catalyst.[7b] This result is further indicative of the advantages of the present catalytic scheme to prepare crystalline nanomaterials using PMOs as templates.

Conclusions

Highly ordered methylene-bridged periodic mesoporous organosilicas with SBA-15 structures (PMO-Me) were

(44) Hanrath, T.; Korgel, B. A. *J. Am. Chem. Soc.* **2002**, *124*, 1424.

(45) (a) Wagner, R. S.; Ellis, W. C. *Appl. Phys. Lett.* **1964**, *4*, 89. (b) Wagner, R. S.; Ellis, W. C.; Jackson, K. A.; Arnold, S. M. *J. Appl. Phys.* **1964**, *35*, 2993.

(46) (a) Hanranth, T.; Korggel, B. A. *Adv. Mater.* **2003**, *15*, 437. (b) Morales, A. M.; Lieber, C. M. *Science* **1998**, *279*, 208.

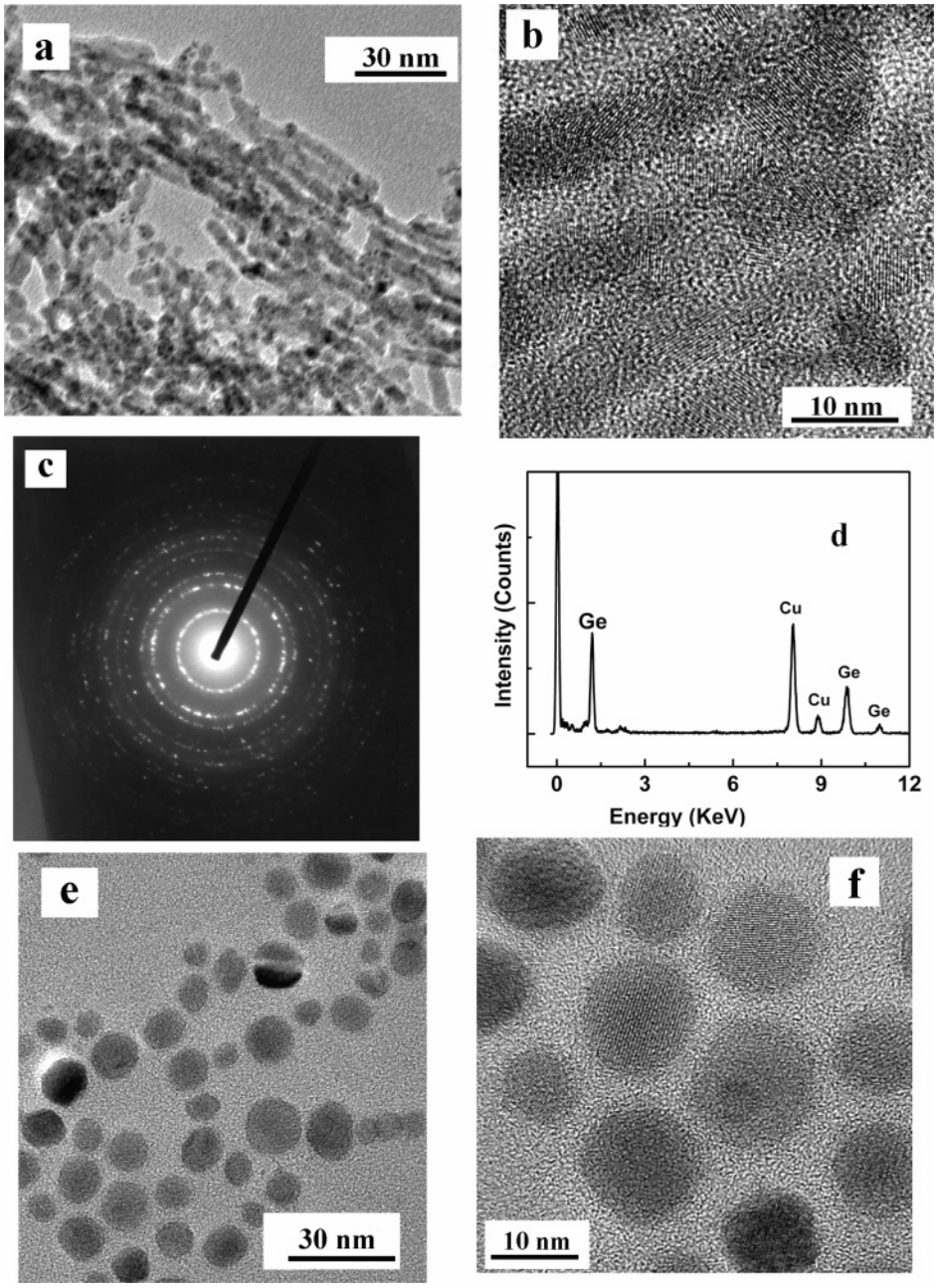

Figure 11. (a) Low magnified TEM images, (b) high-resolution TEM images, (c) electron diffraction (ED) patterns, and (d) EDS of self-supported Ge nanocrystals obtained from Ge-SH-PMO-Me templates. (e) Low magnified TEM images and (f) high-resolution TEM images of the self-supported Ge nanoparticles obtained from Ge-SH-SBA-15.

prepared using P123 as a template under strongly acidic conditions. The PMO-Me samples were functionalized by thiol groups, via an SCF grafting reaction, resulting in bifunctionalized periodic mesoporous organosilicas. Polycrystalline Ge nanomaterials, including nanoparticles and nanorods, have been synthesized within the channels of the SH-PMO-Me materials by a low-temperature catalytic approach. From this study, we conclude that SH-PMO-Me materials are better hosts than mesoporous silicas in the formation of highly crystalline Ge nanocrystals. This result is possibly attributed to the greater hydrophobicity of SH-PMO-Me materials compared to mesoporous silica, making it easier for the Ge precursors to diffuse into, nucleate, and grow inside the pores of the PMOs.

Acknowledgment. The authors acknowledge financial support from the Higher Education Authority (HEA) in Ireland under the PRTLI3 grant scheme, the Irish Research Council for Science Engineering and Technology (IRCSET) for the scholarship awarded to B.D. and CRANN (Polymer Templating Project).

Supporting Information Available: XRD patterns, N_2 sorption isotherms, and pore size distributions of PMO-Me(100), PMO-Me-(80), and PMO-Me(60), XRD pattern of PMO-Me(80) together with that of SH-PMO-Me, and wide-angle XRD patterns of nanoscale Si confined within the pores of SH-PMO-Me and SH-SBA-15 (PDF).This material is available free of charge via the Internet at http://pubs.acs.org.

CM050502H